http://www.TheoryOfEverything.org

3D Polytope Hulls of E_8 4_{21}, 2_{41}, and 1_{42}

J Gregory Moxness*
TheoryOfEverything.org
(Dated: May 19, 2020)

Using rows 2 through 4 of a unimodular 8×8 rotation matrix, the vertices of E_8 4_{21}, 2_{41}, and 1_{42} are projected to 3D and then gathered & tallied into groups by the norm of their projected locations. The resulting Platonic and Archimedean solid 3D structures are then used to study E8's relationship to other research areas, such as sphere packings in Grassmannian spaces, using E_8 Eisenstein Theta Series in recent proofs for optimal 8D and 24D sphere packings, nested lattices, and quantum basis critical parity proofs of the Bell-Kochen-Specker (BKS) theorem.

PACS numbers: 02.20.-a, 02.10.Yn
Keywords: Coxeter groups, root systems, E8

I. INTRODUCTION

This paper will introduce several possible new connections between E_8 4_{21}, 2_{41}, and 1_{42} and the study of sphere packings in Grassmannian spaces[1], using E_8 Eisenstein Theta Series in recent proofs for optimal 8D and 24D sphere packings[2], nested lattices[3], and quantum basis critical parity proofs of the Bell-Kochen-Specker (BKS) theorem[4].

A. Generating Polytopes

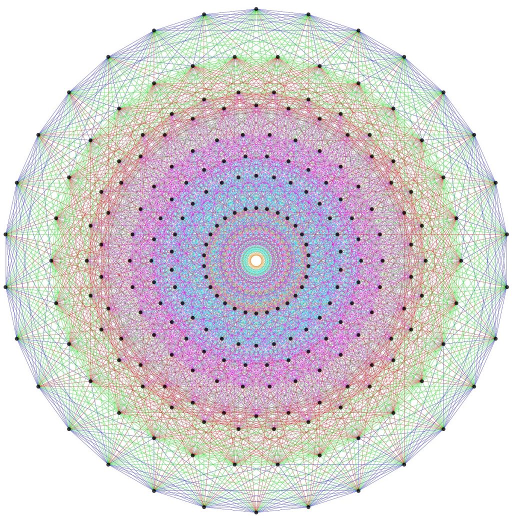

FIG. 1: E_8 4_{21} Petrie projection

Fig. 1 is the Petrie projection of the largest of the exceptional simple Lie algebras, groups and lattices called E_8. The Split Real Even (SRE) form of E_8 has a 4_{21} Gosset polytope of 240 vertices and 6720 edges of 8 dimensional (8D) length $\sqrt{2}$. In addition to this E_8 root polytope identified with the Dynkin diagram shown in Fig. 2a, there are $2^8 - 1 = 255$ possible permutations of the E_8 Dynkin diagram. Several of these other permutations are commonly represented visually using the Petrie projection basis. Among these others are the 2,160 vertex 2_{41} and the 17,280 vertex 1_{42} polytope, which are constructed by generating the resulting roots by moving the ringed (or filled) node to the other ends of the Dynkin diagram, as shown in Figs. 2b and 2c respectively.

Interestingly, E_8 has been shown[5] to fold to the 4D polychora of H_4 (aka. the 120 vertex 720 edge 600-cell) and a scaled copy $H_4\Phi$, where $\Phi = \frac{1}{2}\left(1+\sqrt{5}\right) = 1.618...$ is the big golden ratio and $\varphi = \frac{1}{2}\left(\sqrt{5}-1\right) = 1/\Phi = \Phi - 1 = 0.618...$ is the small golden ratio.

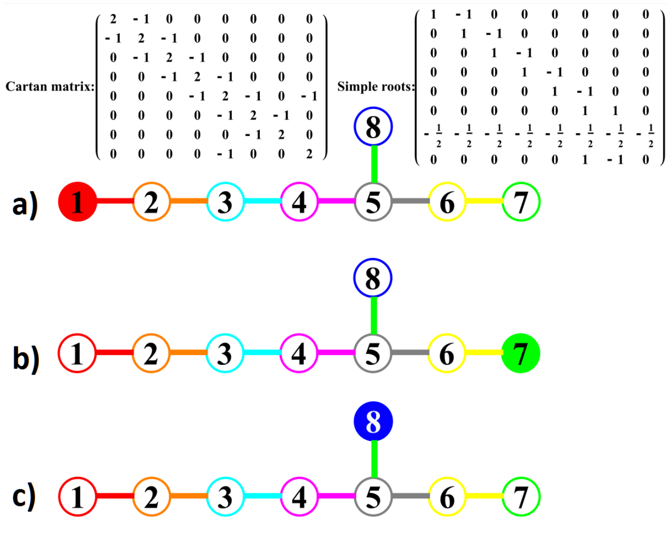

FIG. 2: E_8 Dynkin diagrams a) 4_{21}, b) 2_{41}, c) 1_{42}
Also shown are the Cartan and simple root matrices which correspond to the common Coxeter-Dynkin representation of the diagrams.

*URL: http://www.TheoryOfEverything.org/TOE/JGM; mailto:jgmoxness@TheoryOfEverything.org

B. 8D Platonic Rotation

In a previous paper[6], a unimodular form of a specific matrix for performing an 8D rotation of the SRE E_8 group of root vertices results in the vertices of H_4 (a.k.a. the 600-cell). This rotation (or folding) matrix is related to the Platonic solid icosahedron and was shown to be that of (1).

$$\mathrm{H4_{uni}} =$$

$$\begin{pmatrix} \sqrt{\varphi^3} & 0 & 0 & 0 & \frac{1}{\sqrt{\varphi^3}} & 0 & 0 & 0 \\ 0 & -\sqrt{\varphi} & \frac{1}{\sqrt{\varphi}} & 0 & 0 & \sqrt{\varphi} & \frac{1}{\sqrt{\varphi}} & 0 \\ 0 & \frac{1}{\sqrt{\varphi}} & 0 & -\sqrt{\varphi} & 0 & \frac{1}{\sqrt{\varphi}} & 0 & \sqrt{\varphi} \\ 0 & 0 & -\sqrt{\varphi} & \frac{1}{\sqrt{\varphi}} & 0 & 0 & \sqrt{\varphi} & \frac{1}{\sqrt{\varphi}} \\ \frac{1}{\sqrt{\varphi^3}} & 0 & 0 & 0 & \sqrt{\varphi^3} & 0 & 0 & 0 \\ 0 & \sqrt{\varphi} & \frac{1}{\sqrt{\varphi}} & 0 & 0 & -\sqrt{\varphi} & \frac{1}{\sqrt{\varphi}} & 0 \\ 0 & \frac{1}{\sqrt{\varphi}} & 0 & \sqrt{\varphi} & 0 & \frac{1}{\sqrt{\varphi}} & 0 & -\sqrt{\varphi} \\ 0 & 0 & \sqrt{\varphi} & \frac{1}{\sqrt{\varphi}} & 0 & 0 & -\sqrt{\varphi} & \frac{1}{\sqrt{\varphi}} \end{pmatrix} /2 \tag{1}$$

More interestingly from [7], $H4_{\mathrm{uni}}$ can be generated using a combination of the unitary Hermitian matrices commonly used for Quantum Computing (QC) qubit logic, namely those of the 2 qubit CNOT (2) and SWAP (3) gates. Taking these patterns, combined with the recursive functions that build Φ from the Fibonacci sequence, it is straightforward to derive $H4_{\mathrm{uni}}$ from scaled QC logic gates. $H4_{\mathrm{uni}}$ is shown in Fig. 3.

$$\mathrm{CNOT} = \begin{pmatrix} 1 & 0 & 0 & 0 \\ 0 & 1 & 0 & 0 \\ 0 & 0 & 0 & 1 \\ 0 & 0 & 1 & 0 \end{pmatrix} \tag{2}$$

$$\mathrm{SWAP} = \begin{pmatrix} 1 & 0 & 0 & 0 \\ 0 & 0 & 1 & 0 \\ 0 & 1 & 0 & 0 \\ 0 & 0 & 0 & 1 \end{pmatrix} \tag{3}$$

C. 2D and 3D Projection

Projection of E_8 to 2D (or 3D) requires 2 (or 3) basis vectors $\{X, Y, Z\}$. For the Petrie projection shown in Fig. 1, we start with the basis vectors in (4), which are simply the two 2D Petrie projection basis vectors of the 600-cell (a.k.a. the Van Oss projection), with a 3rd (z) basis vector added for the 3D projection.

$$\begin{array}{llllll} \mathrm{x}=\{ & 0, & \Phi 2\mathrm{Sin}\frac{2\pi}{15}, & 2\mathrm{Sin}\frac{2\pi}{15}, & 0, & 0,0,0,0\} \\ \mathrm{y}=\{ & -\Phi 2\mathrm{Sin}\frac{2\pi}{30}, & 0, & 0, & 1, & 0,0,0,0\} \\ \mathrm{z}=\{ & 1, & 0, & 0, & \Phi 2\mathrm{Sin}\frac{2\pi}{30}, & 0,0,0,0\} \end{array} \tag{4}$$

```
N[H4Uni]
```

$$\begin{pmatrix} 0.242934 & 0. & 0. & 0. & 1.02909 & 0. & 0. & 0. \\ 0. & -0.393076 & 0.63601 & 0. & 0. & 0.393076 & 0.63601 & 0. \\ 0. & 0.63601 & 0. & -0.393076 & 0. & 0.63601 & 0. & 0.393076 \\ 0. & 0. & -0.393076 & 0.63601 & 0. & 0. & 0.393076 & 0.63601 \\ 1.02909 & 0. & 0. & 0. & 0.242934 & 0. & 0. & 0. \\ 0. & 0.393076 & 0.63601 & 0. & 0. & -0.393076 & 0.63601 & 0. \\ 0. & 0.63601 & 0. & 0.393076 & 0. & 0.63601 & 0. & -0.393076 \\ 0. & 0. & 0.393076 & 0.63601 & 0. & 0. & -0.393076 & 0.63601 \end{pmatrix}$$

```
Det@C600
```

$$\frac{9\,437\,184 + 4\,194\,304\sqrt{5}}{16\,384\left(1+\sqrt{5}\right)^6}$$

```
N@%
```

1.

FIG. 3: Numeric $\mathrm{H4_{fold}}$ from the 2 Qubit CNOT and SWAP QC gates and an integer Fibonacci series function output after $n = 20$ iterations
Also shown are the symbolic and numeric calculation for its determinant verifying unimodularity.

$\{X, Y, Z\} = \mathrm{H4_{uni}^{-1}}.\{x, y, z\}$ as shown in (5).

$$\begin{array}{lllllllll} \mathrm{X}=\{ & 0 & .782 & .428 & .32 & 0 & .253 & 0.428 & -.32\} \\ \mathrm{Y}=\{ & -.348 & 0 & .393 & .636 & -.082 & 0 & -.393 & .636\} \\ \mathrm{Z}=\{ & 1.029 & 0 & .133 & .215 & 0.243 & 0 & -.133 & .215\} \end{array} \tag{5}$$

The vertices of each permutation of E_8 used in this document are generated from the code shown in Fig. 8 of Appendix A.

Figs. 9-11 in Appendix B show various 2D projections of 4_{21}, 2_{41}, and 1_{42}. The 7^{th} projection "$E_8 \to H_4$" is the same as that used for what is described in the next section as the "Platonic Projection Prism". The symbolic form of its basis vectors are shown in (6).

D. 3D Platonic Solid Projection Prism

While 3D projections can be generated for each set of basis vectors used in Appendix B, there are only a few that render interesting 3D structures. A few of these are presented in Appendix C Figs. 12-13.

The most interesting 3D projections are found in Figs. 14-18 in Appendix C showing various projections of 4_{21}, 2_{41}, and 1_{42} whch are based on "E8→H4". This basis is derived from the Platonic solid icosahedron. The twelve vertices of the icosahedron can be decomposed into three mutually-perpendicular golden rectangles (as shown in Fig. 4), whose boundaries are linked in the pattern of the Borromean rings. Rows (or columns) 2-4 (or 5-8) of $\mathrm{H4_{uni}}$ contain 6 of the 12 vertices of this icosahedron, including 2 at the origin with the other 6 of 12 icosahedron vertices being the antipodal reflection of these through the origin. These 2 (or 3) rows are then used as a kind of "Platonic solid projection prism" to form the 2 (or 3) 8D basis vectors used in the 2D (or 3D) projection 4_{21}, 2_{41}, and 1_{42}.

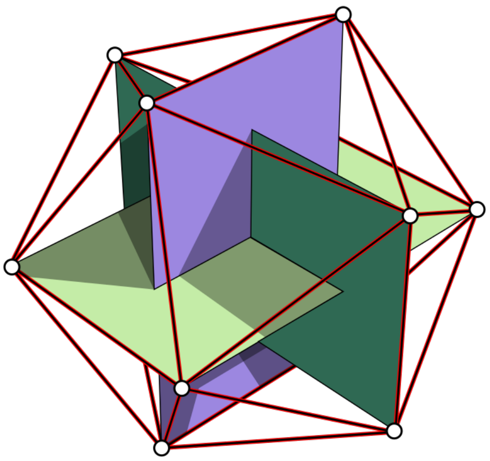

FIG. 4: The icosahedron formed from 3 mutually-perpendicular golden rectangles

$$
\begin{array}{lllllllll}
\text{X=}\{0 & -\frac{\sqrt{2}}{\sqrt{5}+3} & \frac{\sqrt{2}}{\sqrt{5}+1} & 0 & 0 & \frac{\sqrt{2}}{\sqrt{5}+3} & \frac{\sqrt{2}}{\sqrt{5}+1} & 0\} \\
\text{Y=}\{0 & \frac{\sqrt{2}}{\sqrt{5}+1} & 0 & -\frac{\sqrt{2}}{\sqrt{5}+3} & 0 & \frac{\sqrt{2}}{\sqrt{5}+1} & 0 & \frac{\sqrt{2}}{\sqrt{5}+3}\} \\
\text{Z=}\{0 & 0 & -\frac{\sqrt{2}}{\sqrt{5}+3} & \frac{\sqrt{2}}{\sqrt{5}+1} & 0 & 0 & \frac{\sqrt{2}}{\sqrt{5}+3} & \frac{\sqrt{2}}{\sqrt{5}+1}\}
\end{array} \tag{6}
$$

This Platonic solid projection in 3D manifests a large number of concentric hulls with Platonic and Archimedean solid related structures. The 8 hull 4_{21}, which includes two 4 hull 600-cell structures (H_4 & $H_4\Phi$), is shown in Fig. 5. The much larger sets of 2_{41} and 1_{42} are shown in Appendix C Figs. 14-16.

For example, the 3^{rd} largest of 74 hulls in 1_{42} is a pair of overlapping 60 vertex rhombicosidodecahedrons shown in more detail here in Fig. 6. It is an Archimedean solid, one of thirteen convex isogonal nonprismatic solids. The 4th largest hull is a 120 vertex non-uniform truncated icosidodecahedron shown in Fig. 7.

II. PLATONIC LINK TO SPHERE PACKINGS

Fig. 5 of [1] shows a geometric structure with 110 antipodal points from the union of the vertex sets of a dodecahedron (20), an icosidodecahedron (30), and a truncated icosahedron (60). This is structurally the same as that shown in Fig. 18b & 18c without the icosahedron that centers on the pentagons of the truncated icosahedron. The other difference is in the fact that the truncation of the icosahedron in the E_8 projection is not regular and results in a non-uniform rhombicosihedron as shown in Figs. 17a and 18b.

These figures use only the outer two hulls of 4_{21}, 2_{41}, and 1_{42}. The smaller of each of these three pairs of hulls are scaled up to unit norm. For $4_{21} = 2_{41}$, the scale factor used on the overlapping pair of icosahedrons is

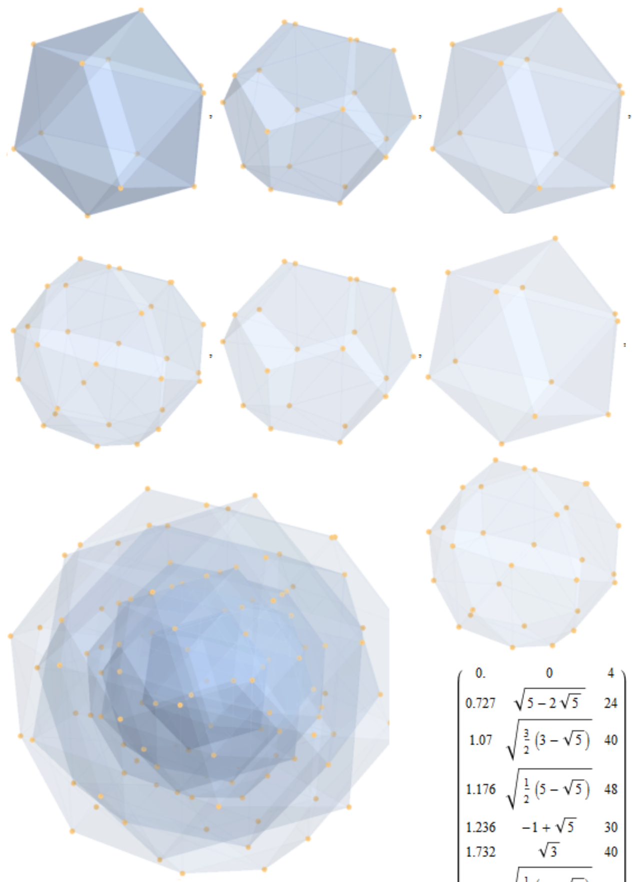

$$
\begin{pmatrix}
0. & 0 & 4 \\
0.727 & \sqrt{5-2\sqrt{5}} & 24 \\
1.07 & \sqrt{\frac{3}{2}\left(3-\sqrt{5}\right)} & 40 \\
1.176 & \sqrt{\frac{1}{2}\left(5-\sqrt{5}\right)} & 48 \\
1.236 & -1+\sqrt{5} & 30 \\
1.732 & \sqrt{3} & 40 \\
1.902 & \sqrt{\frac{1}{2}\left(5+\sqrt{5}\right)} & 24 \\
2. & 2 & 30
\end{pmatrix}
$$

FIG. 5: Individual and grouped concentric hulls of 4_{21} in Platonic 3D projection with numeric and symbolic norm distances and vertex count in increasing opacity

$\sqrt{(8/(5+\sqrt{5}))} \simeq 1.0514$. For 1_{42}, the scale factor used on the overlapping pair of dodecahedrons is $\sqrt{\frac{16+\frac{32}{\sqrt{5}}}{15+\frac{33}{\sqrt{5}}}} \simeq 1.0092$.

It would be interesting to calculate the sphere packing efficiencies of the geometries shown in Fig. 18 as well as those individual hulls showon in Figs. 14-15. While it is straight forward to calculate the projected vertex positions given the information in this paper, these are available in a *Mathematica*™ notebook that is available on the author's website `http://www.TheoryOfEverything.org/TOE/JGM/3D-Polytope-Hulls-of-E8.nb`.

Also related to sphere packings, it was recently proven[2] that the E_8 root lattice and the Leech lattice are universally optimal among point configurations in Euclidean spaces of dimensions 8 and 24, respectively. The proof relies on the use Laplace transforms of quasimodular forms related to the Eisenstein $E_4(q)$ Series integers that are the Theta series of the E_8 lattice. This series from `http://oeis.org/A004009` is

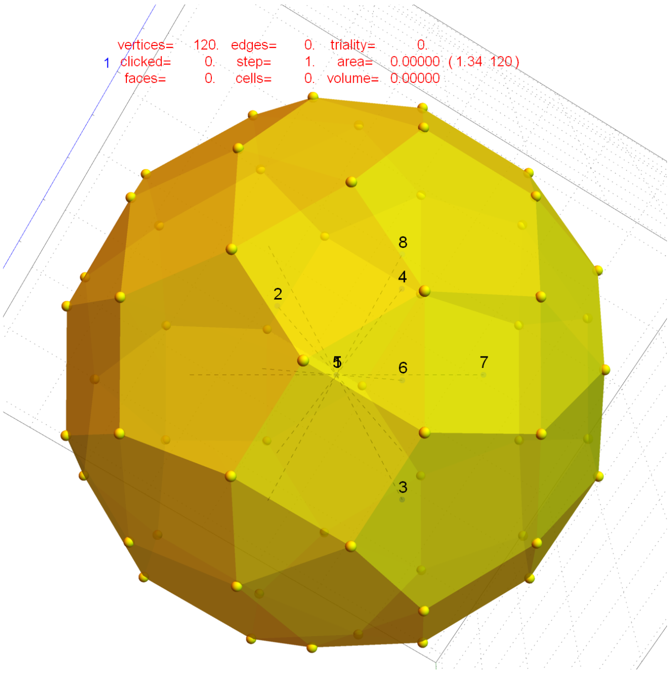

FIG. 6: Pair of overlapping rhombicosidodecahedrons from 3^{rd} largest hull of the 74 hulls in 1_{42}

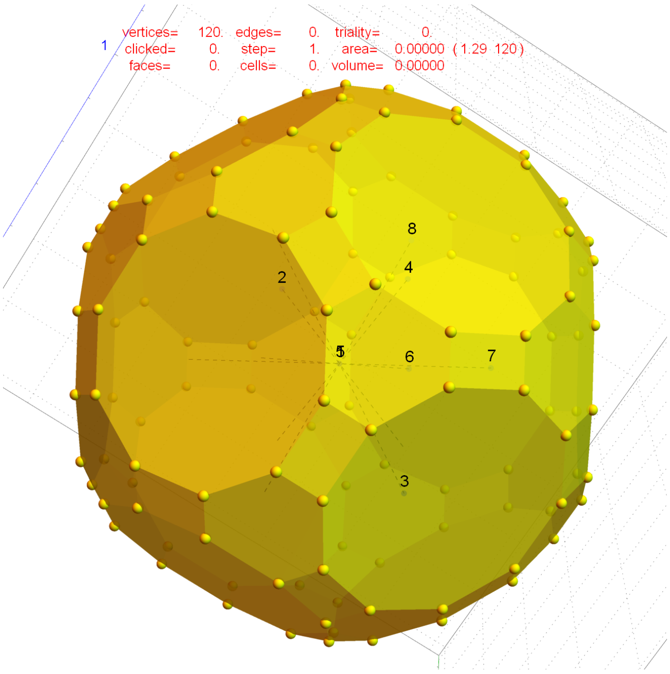

FIG. 7: Non-uniform truncated icosidodecahedrons from 4^{th} largest hull of the 74 hulls in 1_{42}

$\{1, 240, 2160, 6720, 17520, 30240, ...6026880\}$, noting that the 4^{th} term is the number of edges in 4_{21}, and the 5^{th} term is the number of 7-facets in 2_{41}, specifically 240 2_{31} polytopes and 17,280 7-simplices.

III. PLATONIC LINK TO NESTED LATTICES

Also related to E_8's Gossett and Witting polytopes and the aforementioned 4_{21} and 2_{41} Dynkin diagram permutations, a blog article on nested lattices[3] credits Warren D. Smith with observing that the sum of the first three terms in the Theta Series of E_8 is a perfect fourth power $1 + 240 + 2160 = 2401 = 7^4$. The vertices of the related E_8 groups in this series 4_{21} and 2_{41} have been visualized in Figs. 9-10 of Appendix B. The 2160 vertex 2_{41} is also visualized in 3D in Figs. 12 and 14.

IV. PLATONIC LINK TO BELL-KOCHEN-SPECKER (BKS) PARITY PROOFS

The 4D 120 vertex 600-cell (H_4) has been shown[5] to be easily generated by using $H4_{\text{uni}}$ in (1) to rotate $E_8 \to H_4$. The dual 3D Platonic solid structure of icosahedrons and dodecahedrons (embeded in the rhombic triacontahedron) are contained within the 120 vertex 4D 600-cell, itself a combination of the self-dual 24-cells (i.e. 8-cell aka. the tesseract or hyper-cube and the 16-cell orthoplex or cross polytope). Indeed, it has been shown[8] that the 3D Platonic solid structures can be a generator of H_4.

In $\mathbb{CP}^3$, the Penrose dodecahedron of the BKS theorem and the Witting polytope, which is the Complex 4D representation of the SRE E_8 used herein, are shown to be identical[9]. This same structure has been linked to the Bell-Kochen-Specker (BKS) parity proofs[4].

It would be interesting to calculate the proofs from the geometries shown in Fig. 18 as well as those individual hulls showon in Figs. 14-15.

V. CONCLUSION

This paper has introduced new visualizations and connections between E_8 4_{21}, 2_{41}, and 1_{42} and the study of sphere packings in Grassmannian spaces[1], sphere packing proofs using E_8 Eisenstein Theta Series for optimal packing in 8D and 24D, nested lattices, and quantum basis critical parity proofs of the Bell-Kochen-Specker (BKS) theorem. It is anticipated that these visualizations and connections will be useful in discovering new insights into unifying the mathematical symmetries as related to unification in theoretical physics.

Acknowledgments

I would like to thank my wife for her love and patience and those in academia who have taken the time to review this work.

[1] J. H. Conway, R. H. Hardin, and N. J. A. Sloane, *Packing lines, planes, etc.: Packings in grassmannian space* (2002), math/0208004.
[2] H. Cohn, A. Kumar, S. D. Miller, D. Radchenko, and M. Viazovska, *Universal optimality of the e_8 and leech lattices and interpolation formulas* (2019), 1902.05438.
[3] A. P. Goucher, `cp4space.wordpress.com/2020/05/03/nested-lattices/` (2020).
[4] M. Waegell, P. K. Aravind, N. D. Megill, and M. Pavičić, Foundations of Physics **41**, 883–904 (2011), ISSN 1572-9516, URL `http://dx.doi.org/10.1007/s10701-011-9534-7`.
[5] J. G. Moxness, `www.vixra.org/abs/1411.0130` (2014).
[6] J. G. Moxness, `www.vixra.org/abs/1804.0065` (2018).
[7] J. G. Moxness, `www.vixra.org/abs/1910.0345` (2019).
[8] P.-P. Dechant, Proceedings of the Royal Society of London Series A **472**, 20150504 (2016), 1602.05985.
[9] M. Waegell and P. Aravind, Physics Letters A **381**, 1853–1857 (2017), ISSN 0375-9601, URL `http://dx.doi.org/10.1016/j.physleta.2017.03.039`.

Appendix A: *Mathematica^{TM} code to generate the vertex sets* 4_{21}, 2_{41}, *and* 1_{42}

```
(* Permutation functions *)
pm@n_ := Flatten[Outer[List, Sequence @@ Table[{-1, 1}, {n}]], n - 1];
perms8[{a_, b_, c_, d_, e_, f_, g_, h_}] := Flatten[Permutations@{a #1, b #2, c #3, d #4, e #5, f #6, g #7, h #8} & @@@ pm@8, 1];
Eperms8@in_ := Select[perms8@in, EvenQ@Count[Sign@#, -1] &];
(* E8 1_42 vertices *)
e8142 = Union@Join[perms8@{4, 2, 2, 2, 2, 0, 0, 0},
     Flatten[Eperms8@# & /@ {
        {2, 2, 2, 2, 2, 2, 2, 2},
        {5, 1, 1, 1, 1, 1, 1, 1},
        {3, 3, 3, 1, 1, 1, 1, 1}}, 1]] / 4;
Length@%
17280
(* Even to Odd permutations in the last digit          *)
e8142 =  If[Total@Abs@e8142[[#]] == 3, e8142[[#]], ReplacePart[e8142[[#]], 8 → -e8142[[#, 8]]]] & /@ Range@Length@e8142;
(* E8 2_41 vertices *)
e8241 = Union@Join[
     perms8[{1, 0, 0, 0, 0, 0, 0, 0} 4],
     perms8[{1, 1, 1, 1, 0, 0, 0, 0} 2],
     Eperms8[({2, 0, 0, 0, 0, 0, 0, 0} + 1)]] / 4;
Length@%
2160
(* Even to Odd permutations in the last digit          *)
e8241 = (**) √2 (**) If[Total@Abs@e8241[[#]] > 2, ReplacePart[e8241[[#]], 8 → -e8241[[#, 8]]], e8241[[#]]] & /@ Range@Length@e8241;

(* E8 4_21 vertices scaled for Max Norm=1 from Unimodular C600 and it's 3D E8→H4 projection basis *)
e8421 = (**) Φ (**) Union@Join[Eperms8@{1, 1, 1, 1, 1, 1, 1, 1} / 2, perms8@{1, 1, 0, 0, 0, 0, 0, 0}] (**) / √2 (**);
Length@%
240
```

FIG. 8: *Mathematica*$^{\rm TM}$ code to generate the vertex sets 4_{21}, 2_{41}, and 1_{42}

Appendix B: *Various 2D projections of* 4_{21}, 2_{41}, *and* 1_{42}

Figs. 9-11

Appendix C: *Various 3D projections of* 4_{21}, 2_{41}, *and* 1_{42}

Figs. 12-18

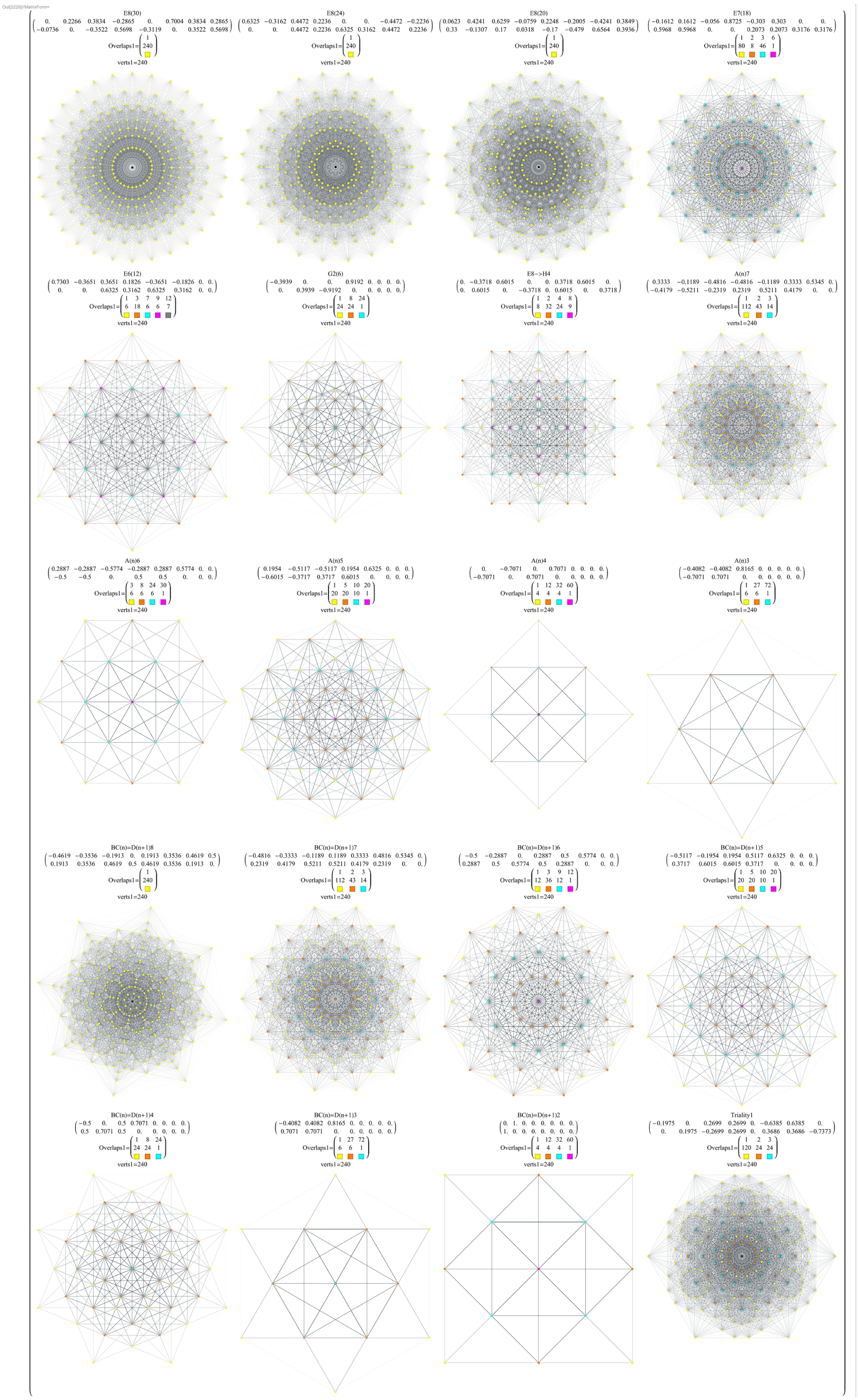

FIG. 9: 4_{21} Polytope projected to various planes
Each 2D projection shown lists the projection name, the numeric basis vectors used, and the 4_{21} overlap color coded vertex groups, and the projection with vertices & 6720 edges

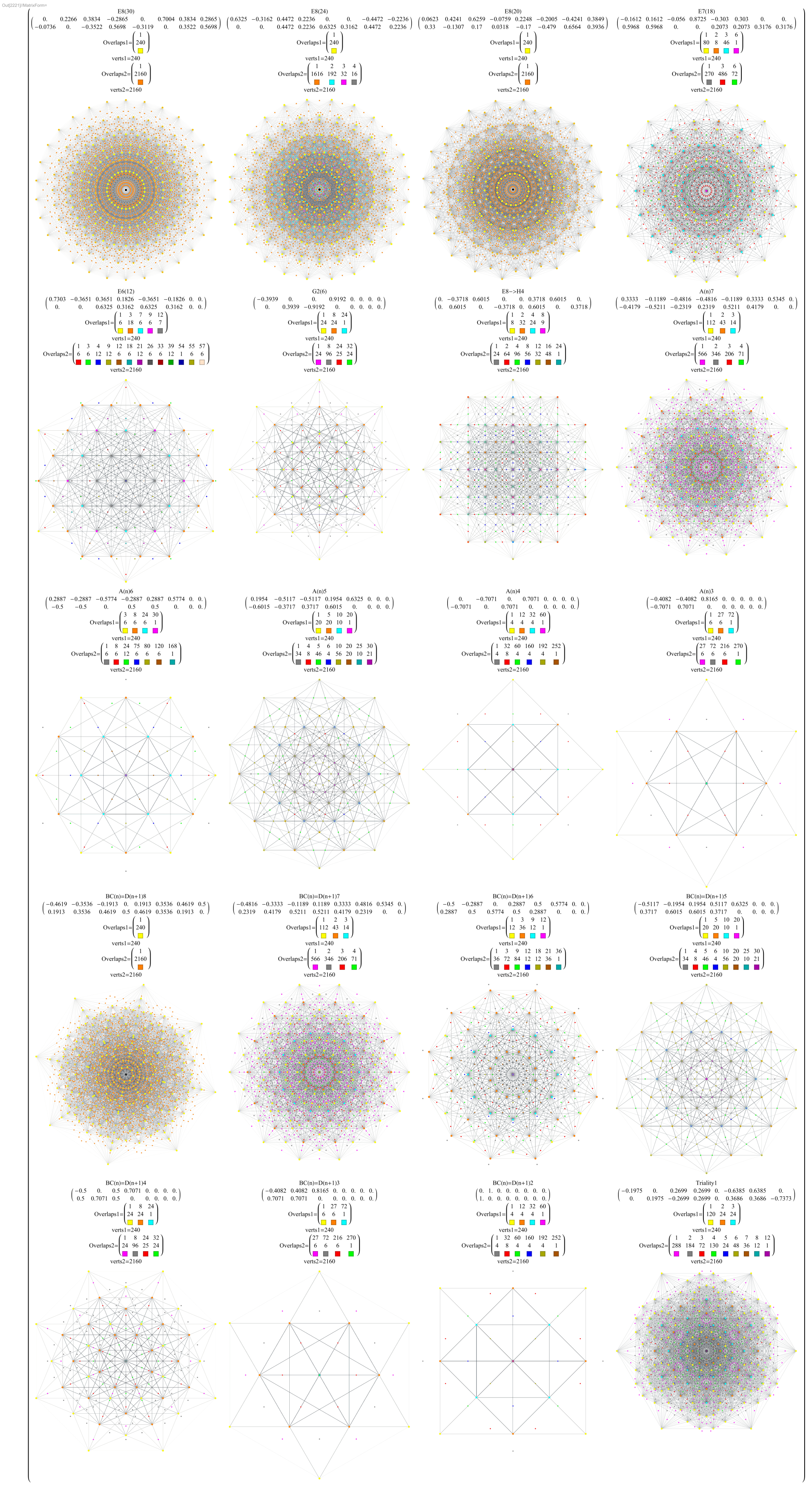

FIG. 10: 4_{21} Polytope projected to various planes
Each 2D projection shown lists the projection name, the numeric basis vectors used, and the 4_{21} & 2_{41} overlap color coded vertex groups, and the projection with vertices (larger) & 6720 edges and the 2_{41} vertices (smaller)

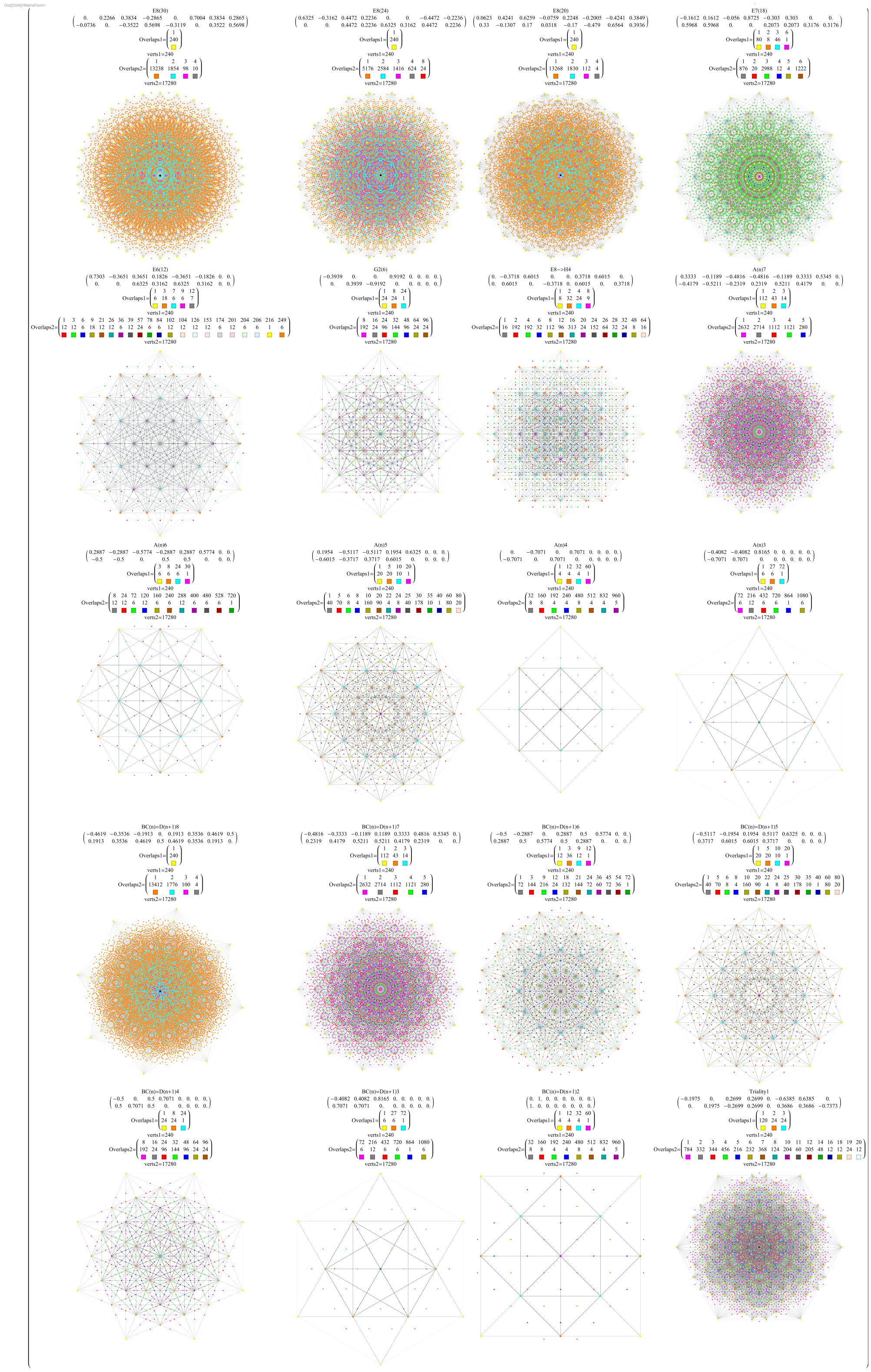

FIG. 11: 4_{21} Polytope projected to various planes
Each 2D projection shown lists the projection name, the numeric basis vectors used, and the 4_{21} & 1_{42} overlap color coded vertex groups, and the projection with vertices (larger) & 6720 edges and the 1_{42} vertices (smaller)

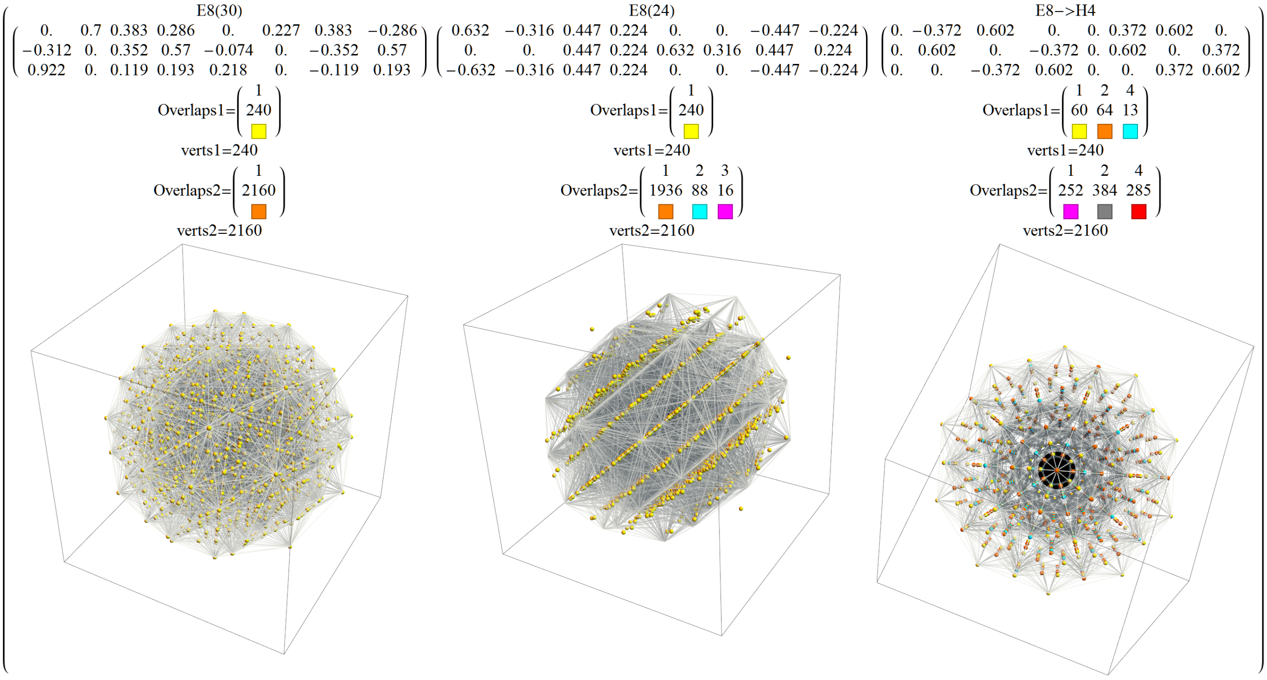

FIG. 12: 4_{21} & Polytope projected to various 3D spaces
Each 3D projection shown lists the projection name, the numeric basis vectors used, and the 4_{21} & 2_{41} overlap color coded vertex groups, and the projection with vertices (larger) & 6720 edges and the 2_{41} vertices (smaller)

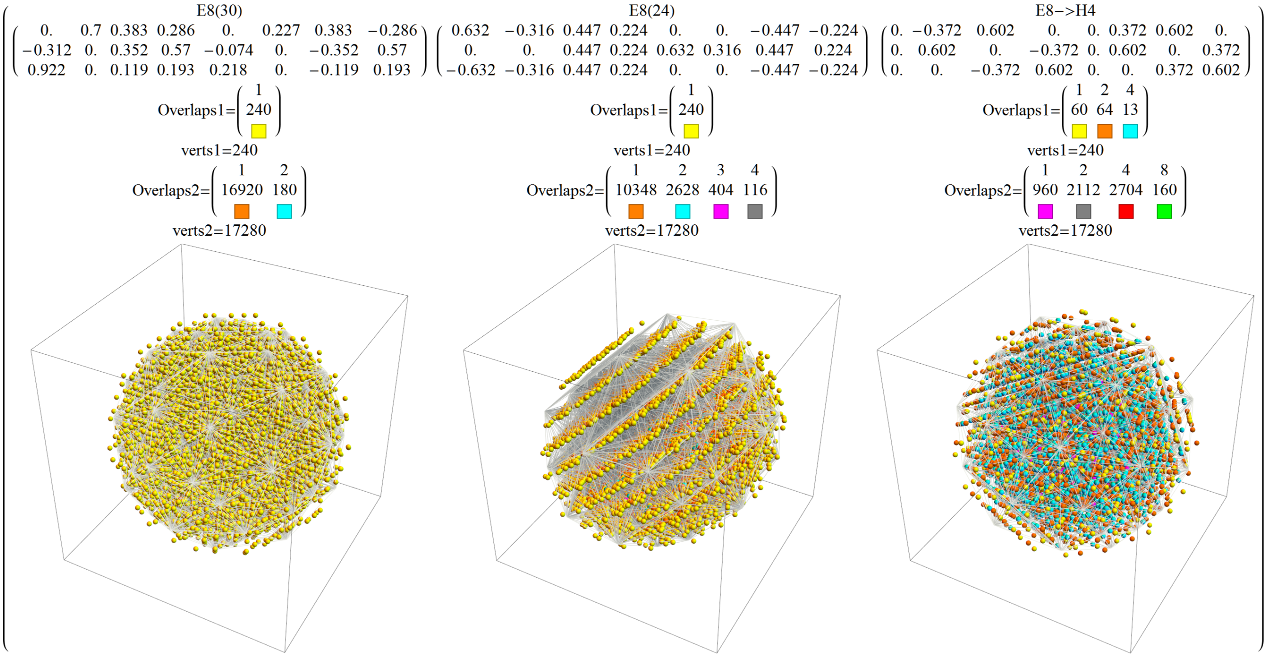

FIG. 13: 4_{21} & Polytope projected to various 3D spaces
Each 3D projection shown lists the projection name, the numeric basis vectors used, and the 4_{21} & 1_{42} overlap color coded vertex groups, and the projection with vertices (larger) & 6720 edges and the 1_{42} vertices (smaller)

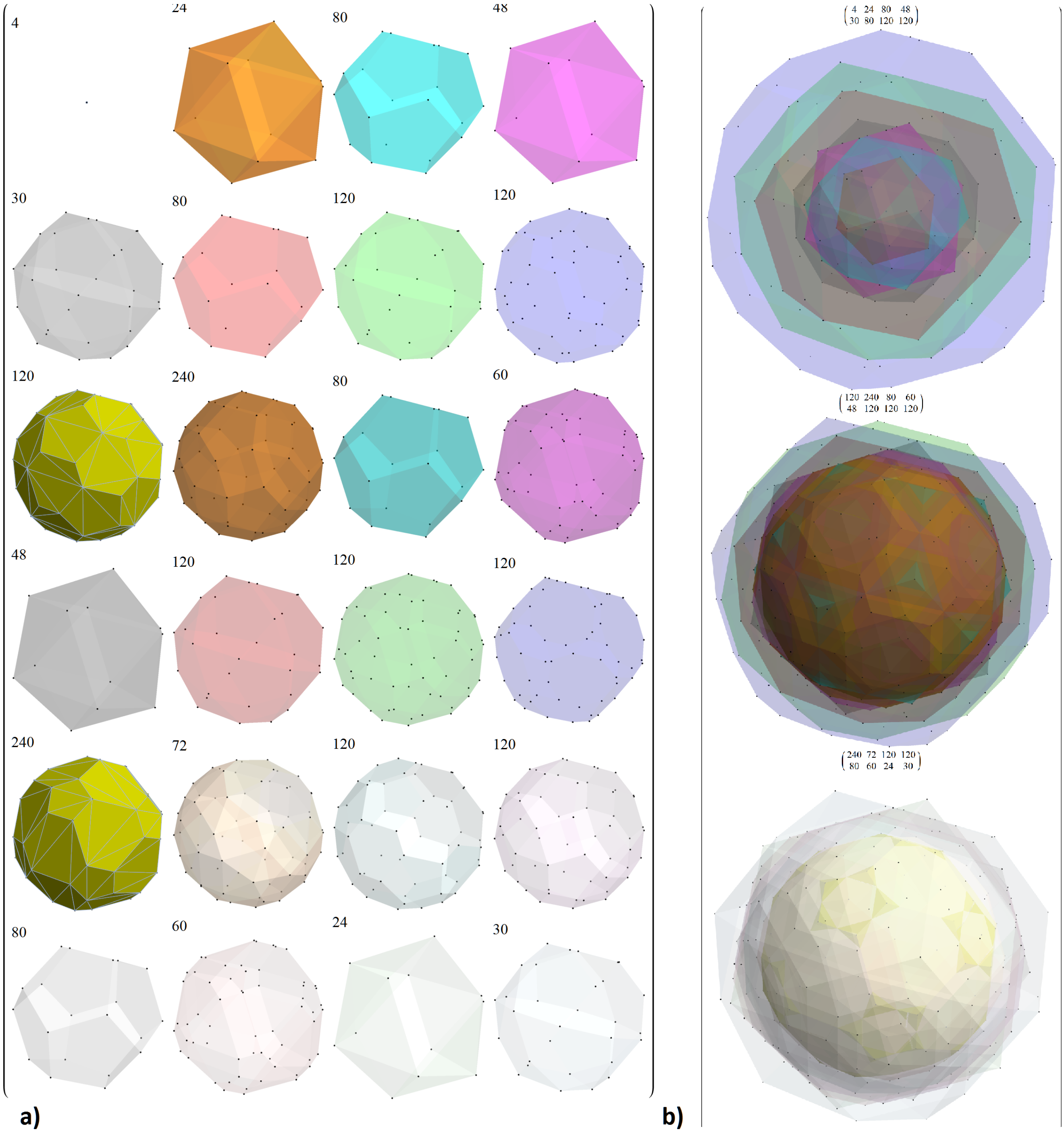

FIG. 14: Concentric hulls of 2_{41} in Platonic 3D projection with vertex count in each hull and increasing opacity and varied surface colors.
a) 24 individual concentric hulls
b) In groups of 8 hulls

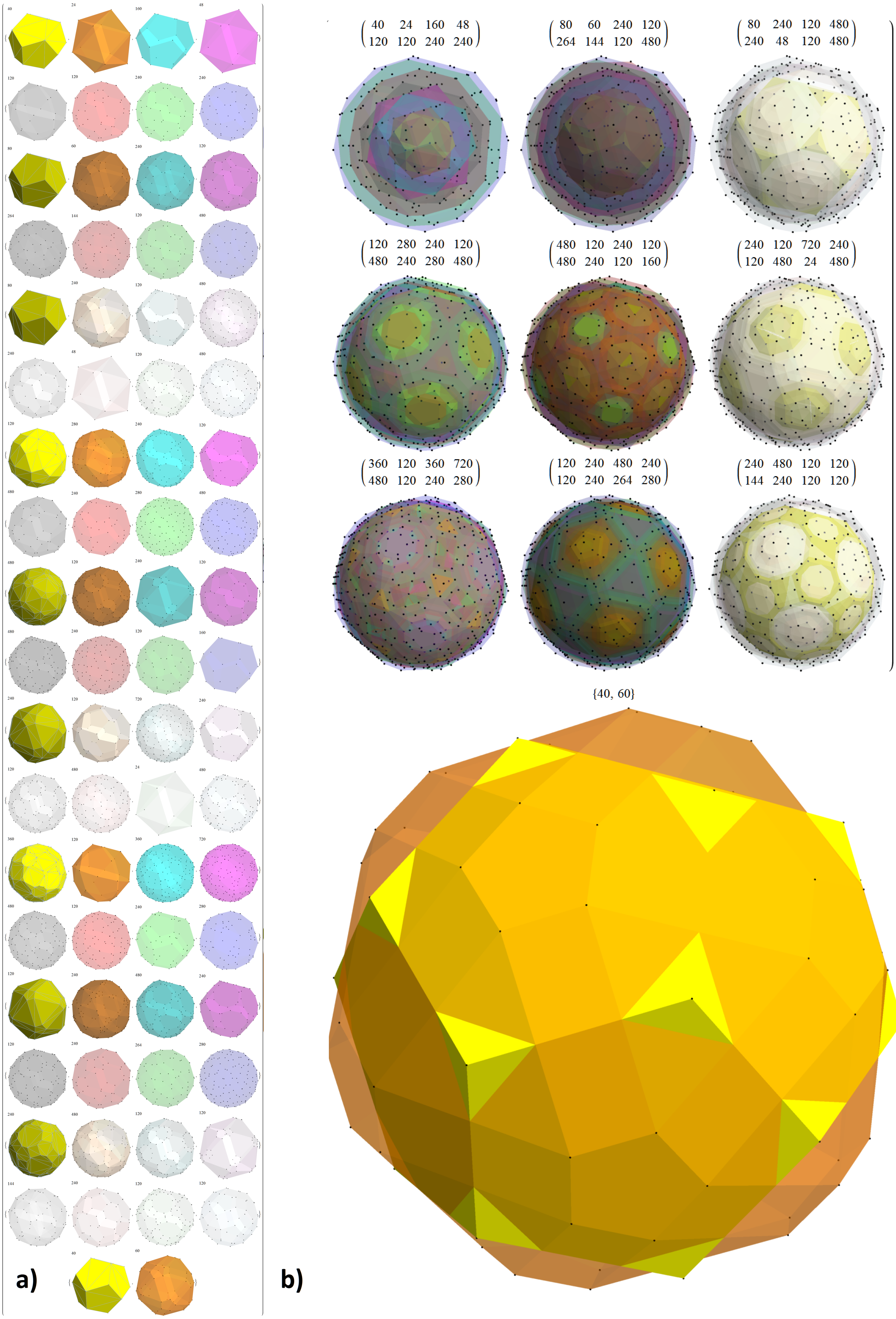

FIG. 15: Concentric hulls of 1_{42} in Platonic 3D projection with vertex count in each hull and increasing opacity and varied surface colors.
a) 74 individual concentric hulls
b) In groups of 8 hulls

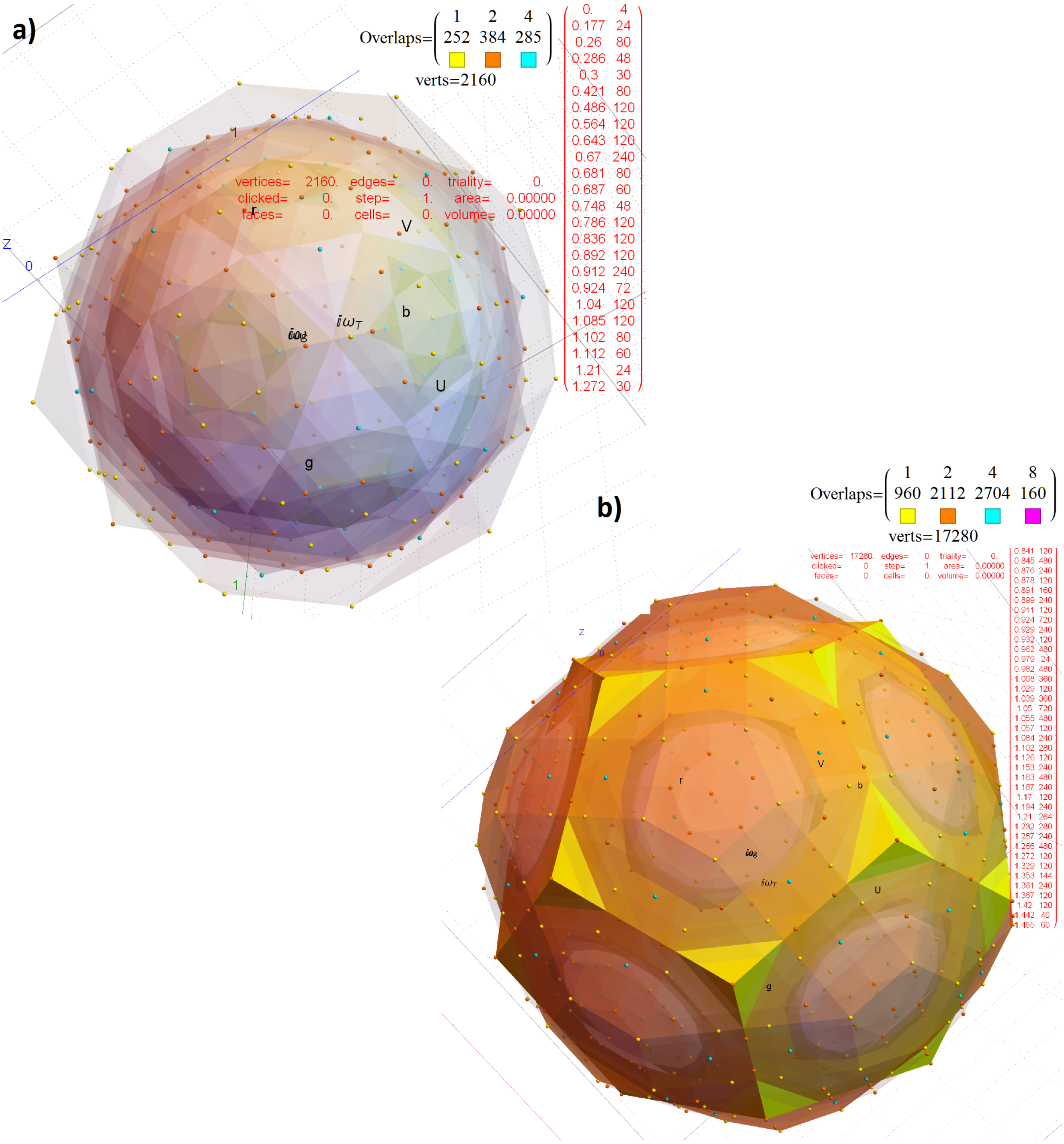

FIG. 16: Combined concentric hulls of 2_{41} and 1_{42} in Platonic 3D projection with increasing opacity and varied surface colors. Also listing grouped vertex counts color coded by overlaps (black text) and norm distances and vertex counts (red text).
a) 24 hulls of 2_{41}
b) 74 hulls of 1_{42}

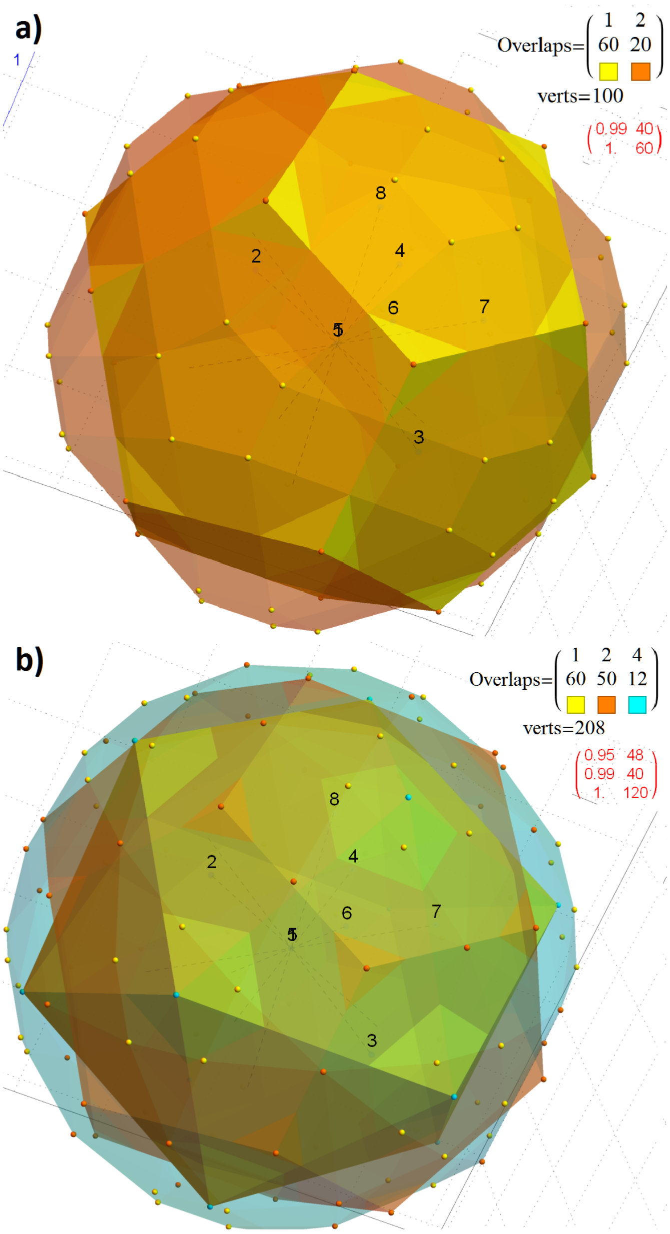

FIG. 17: E_8's outer two hulls scaled to unit norms in Platonic 3D projection with increasing opacity and varied surface colors. Also listing grouped vertex counts color coded by overlaps (black text) and norm distances and vertex counts (red text).
a) 100 vertex 1_{42} non-uniform rhombicosidodecahedron (60 yellow vertices) & two overlapping dodecahedrons (20 red vertices)
b) 208 vertex combination of a, adding two sets of 4_{21}=2_{41} icosidodecahedrons (30 red) & four overlapping icosahedrons (12 cyan vertices)
Note: The internal numbers of the image are the 8 axis (i.e. the projection basis vectors).

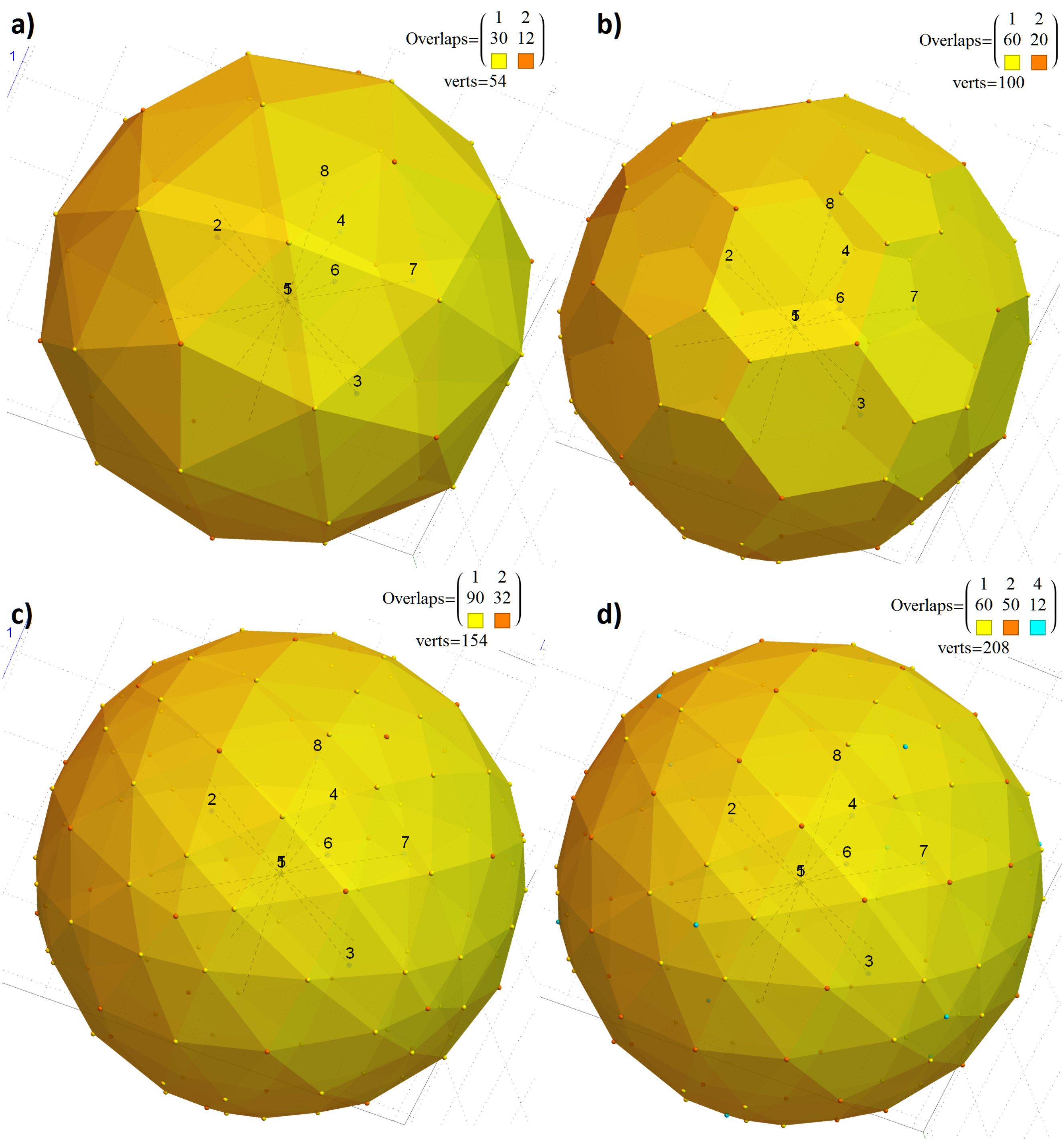

FIG. 18: E_8's outer two hulls scaled to unit norms in Platonic 3D projection with vertex counts color coded by overlaps
a) 54 vertex (42 unique) 4_{21}=2_{41} icosidodecahedron (30 yellow) & two overlapping icosahedrons (12 red) scaled 1.051
b) 100 vertex (80 unique) 1_{42} non-uniform rhombicosidodecahedron (60 yellow) & two overlapping dodecahedrons (20 red) scaled 1.0092
c) 154 vertex (122 unique) combination of a & b
d) 208 vertex (122 unique) combination same as c with color coded vertex counts for both 4_{21} & 2_{41}
Note: The internal numbers of the image are the 8 axis (projection basis vectors).